J Appl Electrochem (2015) 45:343–352
DOI 10.1007/s10800-015-0792-5

RESEARCH ARTICLE

Electrochemical detection of bisphenol A at graphene/melamine nanoparticle-modified glassy carbon electrode

Rongyan Shen · Weiming Zhang · Yuan Yuan · Guangyu He · Haiqun Chen

Received: 10 November 2014 / Accepted: 28 January 2015 / Published online: 8 February 2015

Abstract Due to the unique electronic properties and high adsorption capacity of graphene, a facile strategy was developed to form graphene/melamine nanocomposite by anchoring melamine molecule on the surface of graphene sheets. As the electrostatic attraction happened between protonated melamine and negatively charged bisphenol A (BPA), a novel electrochemical sensor was fabricated to determine the endocrine disruptor BPA by depositing graphene/melamine nanocomposite on the surface of glassy carbon electrode. The electrochemical behavior of BPA was investigated in phosphate buffer solution (pH 7.0) using the prepared sensor. A well-defined anodic peak at 0.56 V was found to attribute to the electrooxidation of BPA on the modified electrode. The kinetic parameters, charge transfer coefficient, electron transfer number, proton transfer number, and standard rate constant were calculated and optimized. The electrochemical sensor exhibited a wider linear range of 1.0×10^{-8} to 2.0×10^{-4} M BPA and a lower detection limit of 4.0×10^{-9} M ($S/N = 3$). This novel sensor was successfully applied to determine BPA leached from real plastic samples with good recoveries ranging from 97.00 to 100.96 %.

Keywords Bisphenol A · Graphene · Melamine · Electrochemical detection · Modified Glassy carbon electrode · Nanoparticle

R. Shen · W. Zhang · Y. Yuan · G. He (✉) · H. Chen (✉)
Key Laboratory of Advanced Catalytic Materials and Technology, Changzhou University,
Changzhou 213164, Jiangsu, People's Republic of China
e-mail: hegy@cczu.edu.cn

H. Chen
e-mail: hqchenyf@hotmail.com

1 Introduction

Bisphenol A (BPA), an important industrial chemical, is mainly used in the production of polycarbonate plastics, epoxy resins, dental sealants, food packaging, etc. Recently, it has received wide attention due to its possible toxicity to health and environmental impacts [1, 2]. Moreover, BPA is one of the typical endocrine-disrupting chemicals (EDCs) which could imitate the biological activity of natural hormones, occupy the hormone receptors, or interfere with the transport and metabolic processes of natural hormones, finally pose a risk to animals and humans [3]. The study from Tufts University Medical School concluded that BPA might increase the risk of cancer [4]. So it is essential to revise and optimize the existing detection methods of BPA. This will help to find reliable tools for risk assessment and reduce the exposure of BPA to human.

Traditional detection methods of BPA include chromatographic techniques coupled with mass spectrometry, capillary electrophoresis, solid-phase microextraction, etc [1, 5, 6]. These methods are time-consuming because the pretreatment of the sample is required and cannot be performed on-site. Electrochemical sensors can provide rapid and on-site detection of BPA [1]. So electrochemical method would be a good alternative as an analytical technique due to its fast response speed, low cost, simple operation, high sensitivity, excellent selectivity, and real-time in situ detection [7–11].

Graphene, a two-dimensional crystal, has aroused wide concern due to its high conductivity, good biocompatibility, electronic property, and potential applications in electrochemical sensors [12–14]. Ntsendwana et al. prepared the glassy carbon electrode (GCE) modified with graphene for the detection of BPA [15]. Wang et al.

fabricated the chitosan and graphene/carbon ionic liquid electrode [16]. The modified electrode was then used to investigate the electrochemical behavior of BPA by cyclic voltammetry. But the preparation of the sensor was cumbersome. Hence, it would be a challenge to fabricate a new uncomplicated electrochemical sensor based on familiar carbon materials with higher sensitivity by incorporating the interaction sites onto the surface of graphene.

Melamine (M), an inexpensive and readily available chemical raw material, is widely used. It has attracted wide attention from researchers in various countries. M has the nitrogen-rich and conjugate structure. Metagenic single and double bonds exist in the cyclic structure of M. This is similar to the benzene ring. Graphene could be non-covalently modified by some organic molecules and conjugated polymers with large conjugated structure. The noncovalent interactions (such as π–π stacking, hydrogen bonding, and electrostatic attraction) can exist between the modifier and graphene. π–π interactions can exist between the delocalized π conjugated systems of graphene oxide and the π electrons in M. Then the functionalized graphene oxide can be obtained. Moreover, the amino groups of M ring were prone to undergo the nucleophilic addition reaction in an alkaline environment.

In this work, we choose M as the modifier. As the pK_a of M is 8.0, the amino groups of M could be protonated at pH 7.0. The protonated M could thus interact with the negatively charged BPA through electrostatic attraction. Reduced graphene oxide (RGO) was functionalized with M to form RGO/M nanocomposite, which was then deposited onto GCE. A highly sensitive electrochemical sensor for the determination of BPA in aqueous solution was obtained. This electrochemical sensor combined the electrocatalytic property of graphene and the electrostatic attraction of protonated M. So it exhibited an attractive ability of highly sensitive detection of BPA in real samples. So far, there is no report on the modification of RGO/M for the determination of BPA. Moreover, the sensor was characterized by a lower detection limit, a wider linear range, and easier operation. GCE modified with RGO/M was superior to those reported in many previous results [17–22].

2 Experimental

2.1 Reagents

Bisphenol A, melamine, graphite, HNO_3, Na_2HPO_4, NaH_2PO_4, and HCl were purchased from Sinopharm Chemical Reagent Co. Ltd. (China). All chemicals and solvents were of analytical grade. Ultrapure water was used in all experiments.

2.2 Apparatus

The morphology of the prepared samples was observed using the field-emission scanning electron microscope (SEM) (Hitachi S-4800, Japan) operated at an accelerating voltage of 5 kV. Fluorescence spectra were recorded at room temperature using the F900 fluorescence spectrometer (Edinburgh Instruments Ltd., United Kingdom). UV–Vis spectra were obtained from the UV2700 UV–Vis Spectrophotometers (Shimadzu Corporation). pH measurements were carried out on the PHBJ-260 digital pH meter (Shanghai Rex Co., Ltd., China). Electrochemical measurements were performed on the CHI 920 workstation (Shanghai Chenhua, China).

2.3 Procedures

2.3.1 Preparation of RGO/M

Graphene oxide (GO) was prepared using graphite powder by the modified Hummers' method [23]. 50 mg GO was dispersed in 50 mL water by ultrasonication for 0.5 h to obtain the yellow–brown dispersion. Unexfoliated GO was removed by centrifugation. The obtained GO was then reduced with hydrazine at 90 °C for 1 h. Then it was washed with deionised water and dried at 60 °C [24]. Equal volumes of RGO suspension (1.0 mg mL^{-1}) and the saturated solution of M (3.3×10^{-6} mg mL^{-1}) were mixed together and ultrasonicated for 30 min to form the RGO/M nanocomposite.

2.3.2 Preparation of RGO/M-GCE

Prior to the surface modification, the bare GCE was polished down to 0.05 μm with alumina slurry. Then it was successively washed with anhydrous alcohol and double-distilled water in an ultrasonic bath and dried at room temperature. 15 μL suspension of RGO/M was cast on the surface of GCE with a microinjector. Then GCE was dried at room temperature to form a stable film. For comparison, GCE modified with RGO (RGO–GCE) was fabricated with the similar procedure. The schematic diagrams for the fabrication of RGO/M-GCE and the electrochemical detection of BPA are shown in Fig. 1.

2.3.3 Electrochemical measurements

The cyclic voltammograms (CV), electrochemical impedance spectroscopy (EIS), chronocoulometry experiments, and differential pulse voltammograms (DPV) were performed using the CHI 920 workstation with the conventional three-electrode system (a platinum wire auxiliary electrode, a saturated calomel electrode as the reference

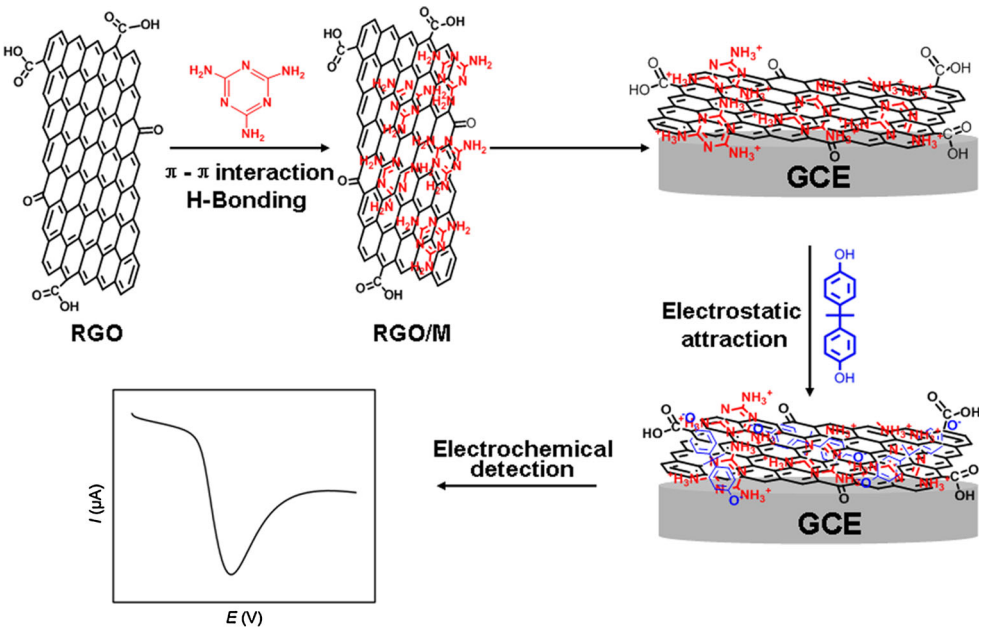

Fig. 1 Schematic diagrams for the fabrication of RGO/M-GCE and the electrochemical detection of BPA

electrode, and the modified or bare working GCE). All measurements were carried out at room temperature.

2.4 Extraction of BPA in samples

BPA was extracted from real samples (PVC food package, PC baby bottle, and PC water bottle) according to the method reported by Kuramitz et al. [25]. Briefly, the sample was cut into pieces (2.00 g), and ultrasonicated for 30 min in 30 mL ultrapure water which was then kept at 70 °C for 48 h in an oil bath. After filtration, the liquid phase was collected in 100 mL flask. The extraction process was repeated three times. Then 4.00 mL of the sample was added into 4.00 mL phosphate buffer (pH 7) and stored at 4 °C before analysis.

3 Results and discussion

3.1 Characterization of RGO/M

The UV–Vis spectroscopy was used to study the functionalization process of RGO. As shown in Fig. 2a, a spiculate peak appeared at 203 nm in the UV–Vis spectrum of M, which was assigned to the π–π^* transitions of the amino groups. RGO showed a strong absorption at 271 nm, which corresponded to the π-conjugation network of the RGO nanosheets. Strong absorption at 271 nm and 203 nm in RGO/M nanocomposite further indicated the immobilization of M on RGO (Fig. 2a).

To investigate the π–π interaction between RGO and M, fluorescence spectra of M and RGO/M suspension were carried out (Fig. 2b). Upon excitation of M at 240 nm, a strong fluorescence emission peak was observed in aqueous solution of M (curve a). However, after M was assembled on RGO, the fluorescence emission excited at 240 nm showed the enhancement of fluorescence. The fluorescence emission peak synchronously increased with the increase of RGO concentration, which attributed to the enlargement of conjugated system. This suggested that the nanocomposites were formed via the noncovalent interaction of π–π between M and the planar structure of RGO. Another reason of fluorescence enhancement arose from the residual carboxyl and hydroxyl groups of RGO integrating with amino groups of M. The fluorescence quenching caused by the amino groups of M was restrained. The fluorescence spectra confirmed that RGO/M was not a simple physical mixture but a nanocomposite in which the planar sheets of GO acted as a good platform for M to be immobilized through electronic interactions.

3.2 Surface morphology of RGO/M

The morphology of RGO/M was investigated by SEM analysis. As shown in Fig. 2c, the RGO/M nanocomposite resembled the crumpled silk veil. This indicated that GO was successfully exfoliated and the molecules of M might be immobilized at the surface of GO so as to form a steric barrier against its agglomeration.

3.3 EIS of RGO/M-GCE

5 mM $[Fe(CN)_6]^{3-/4-}$ solution was used as the electrochemical probes, and AC impedance measurements were

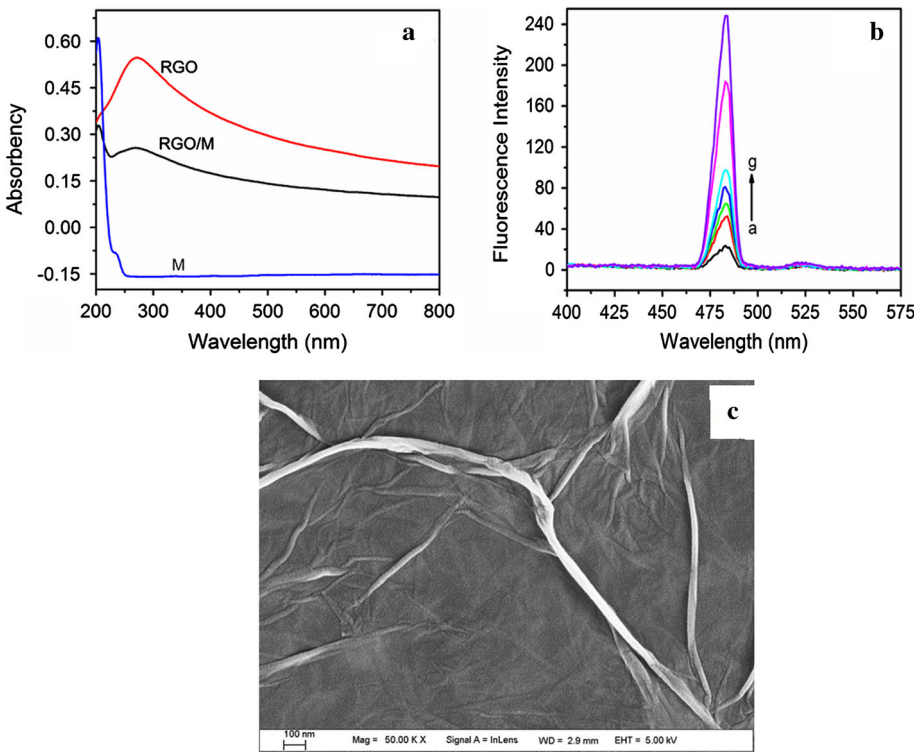

Fig. 2 **a** UV–Vis absorption spectra of M, RGO, and RGO/M. **b** Fluorescence spectra of the saturated aqueous solution of M assembled with RGO (the concentration of RGO is 0, 0.002, 0.004, 0.006, 0.008, 0.016, and 0.032 mg mL^{-1} from *a* to *g*, respectively). **c** SEM image of RGO/M-GCE (100 nm)

conducted in the frequency range of 0.1–100,000 Hz. EIS was employed for further characterization of the modified electrode from 0.3 V to 0.9 V (Fig. 3a). The diameter of semicircle in the Nyquist plot at high frequency corresponded to the electron transfer resistance, which could be calculated according to the equivalent circuit (the insert of Fig. 3). In the high frequency section, certain semicircle was observed for bare GCE (curve a), showing an electron transfer resistance of about 326 Ω. The resistance value dramatically decreased to 20.6 Ω, and the radius obviously became small after the bare electrode was modified with RGO (curve b), which should be attributed to the good conductivity and the large surface area of RGO. This suggested that RGO accelerated the electron transfer between electrochemical probe and the surface of electrode. However, the interfacial electron transfer resistance slightly increased to about 202.2 Ω when RGO/M was immobilized on GCE (curve c). It should be ascribed to the existence of the insulating M. This also indicated that M and RGO were successfully immobilized onto the surface of GCE as a composite RGO/M.

3.4 Characterization of electrochemical behavior of RGO/M-GCE

Electrochemical behavior of the modified electrode was investigated by CV in 0.1 M PBS (pH 7.0). As shown in Fig. 3b, when 2.5×10^{-5} M BPA was added into PBS, a well-defined oxidation peak was observed on all electrodes within the potential window of 0.3–0.9 V. It revealed that the oxidation reaction of BPA was a totally irreversible electrode reaction, which was in agreement with previous reports [26]. On the bare GCE (curve a), a broad oxidation peak was observed at about 0.58 V with a low peak current. The oxidation current of BPA (at 0.55 V) on RGO-GCE (curve b) was higher than that on bare GCE. This indicated that the high surface area and high conductivity of GO increased the effective area of electrode and improved the catalytic activity toward the oxidation of BPA. Compared with the bare GCE and RGO-GCE, a significant enhancement in the anodic current (at 0.56 V) was achieved on the RGO/M-GCE (curve c). This was because that M was protonated at pH 7.0 and became positively charged. Due to the electrostatic attraction, the existence of M enhanced the adsorption of RGO/M toward the negatively charged BPA. Consequently, the oxidation current was increased [27].

3.5 Effects of scan rate

Figure 4 shows that CV curves of 2.5×10^{-5} M BPA on RGO/M-GCE had different scan rates. As shown in Fig. 4a, the oxidation peak current linearly increased with the scan rates in the range of 40–150 mV s^{-1}, and the equation could be expressed as following:

$$I_{pa} = 0.2065v - 3.006(R = 0.9998). \quad (1)$$

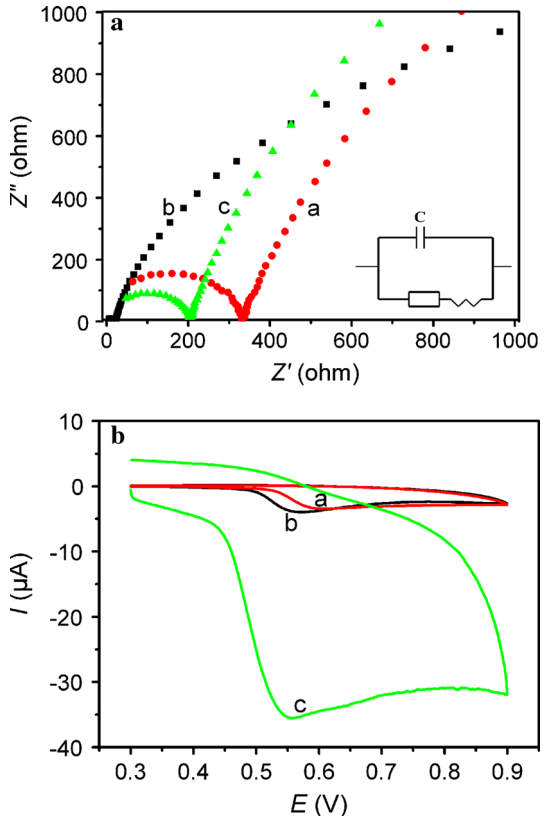

Fig. 3 **a** EIS for bare GCE (*a*), RGO-GCE (*b*), and RGO/M-GCE (*c*) in 0.1 M KCl containing 5 mM $[Fe(CN)_6]^{3-/4-}$ with the sweeping frequency from 10^5 to 0.1 Hz. Inset is the equivalent circuit applied to fit the impedance measurements. **b** CV curves of bare GCE (*a*), RGO-GCE (*b*), and RGO/M-GCE (*c*) in PBS solution containing 25 μM BPA at the scan rate of 50 mV s^{-1}

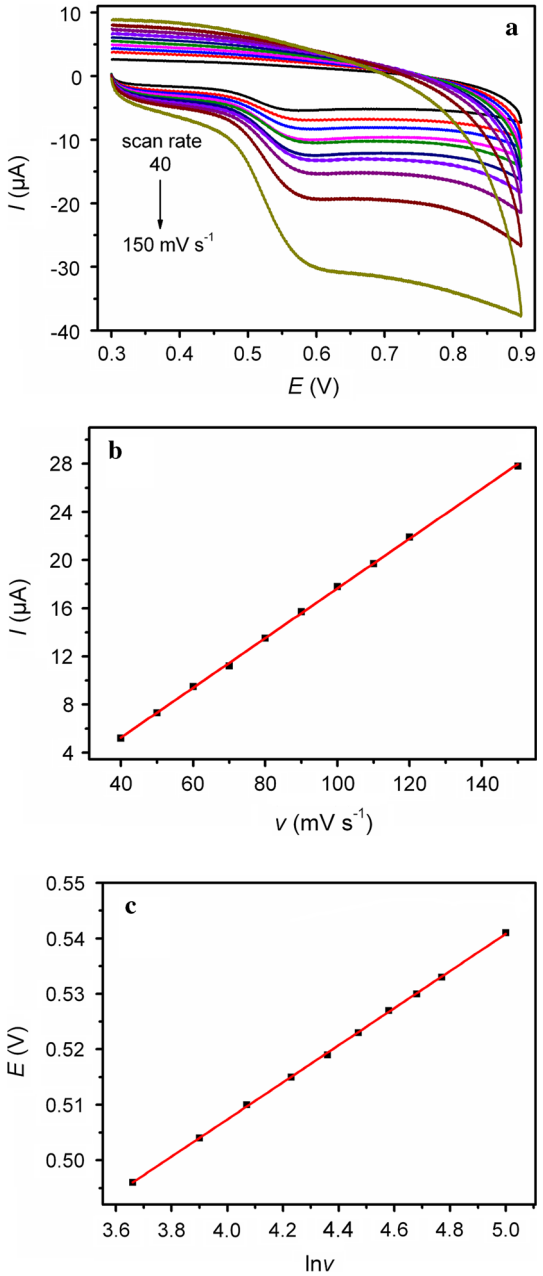

Fig. 4 **a** CV curves of RGO/M-GCE in 0.1 M PBS containing 25 μM BPA at various scan rates (40, 50, 60, 70, 80, 90, 100, 110, 120, and 150 mV s^{-1} from a to j, respectively). **b** The plot of peak current versus scan rate

It indicated that the oxidation of BPA on RGO/M-GCE was a typical adsorption-controlled process (Fig. 4b). Similarly, the linear relationship between E_{pa} and ln v was also observed in the range of 40–150 mV s^{-1} (Fig. 4c). The equation could be expressed as following:

$$E_{pa} = 0.0334 \ln v + 0.3736 (R = 0.9999). \quad (2)$$

For the adsorption-controlled and totally irreversible electrode process [26], E_{pa} was defined by the following equation:

$$E_{pa} = E^0 + (RT/\alpha nF) \ln(RTk^0/\alpha nF) + (RT/\alpha nF) \ln v, \quad (3)$$

where α is the transfer coefficient, k_0 is the standard rate constant of the reaction, n is the electron transfer number involved in the rate-determining step, v is the scan rate, E^0 is the formal redox potential, R is the gas constant, T is the absolute temperature, and F is the Faraday constant. According to the linear correlation of E_{pa} versus ln$v$ (Eq. (2)), the slope of the line was equal to $RT/\alpha nF$. Therefore, αn was calculated to be 0.86. Generally, α was assumed to be 0.5 in totally irreversible electrode process, so the electron transfer number (n) was around 2. As demonstrated in the pH-dependent electrochemical response, the numbers of electron and proton involved in the oxidation process of BPA were equal, and the electrooxidation of BPA on RGO/

M-GCE was the two-electron and two-proton process, which could be illustrated as following:

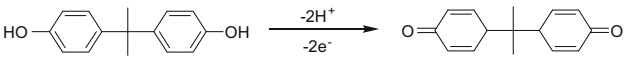

3.6 Effects of accumulation potential and accumulation time

It was generally known that accumulation could improve the amount of BPA adsorbed on the electrode surface. Then the sensitivity of determination was improved, and the detection limit was lowered. The influences of accumulation time along with accumulation potential on the oxidation peak current obtained on the RGO/M-GCE were investigated from 0.3 to 0.9 V. Figure 5a shows that the oxidation peak current gradually increased with the accumulation time. The longer the accumulation time was, the more the BPA inserted to the interlayer of RGO/M and adsorbed onto its surface was. Only slight increase of the peak current was observed after 200 s of accumulation, suggesting that the accumulation of BPA on the modified GCE rapidly reached saturation. Besides, the influence of the accumulation potential on the oxidation peak current of BPA was investigated (Fig. 5b). The highest oxidation peak current was achieved at −0.2 V. Thus, the accumulation step was performed at an optimal accumulation potential of −0.2 V and an optimal accumulation time of 200 s.

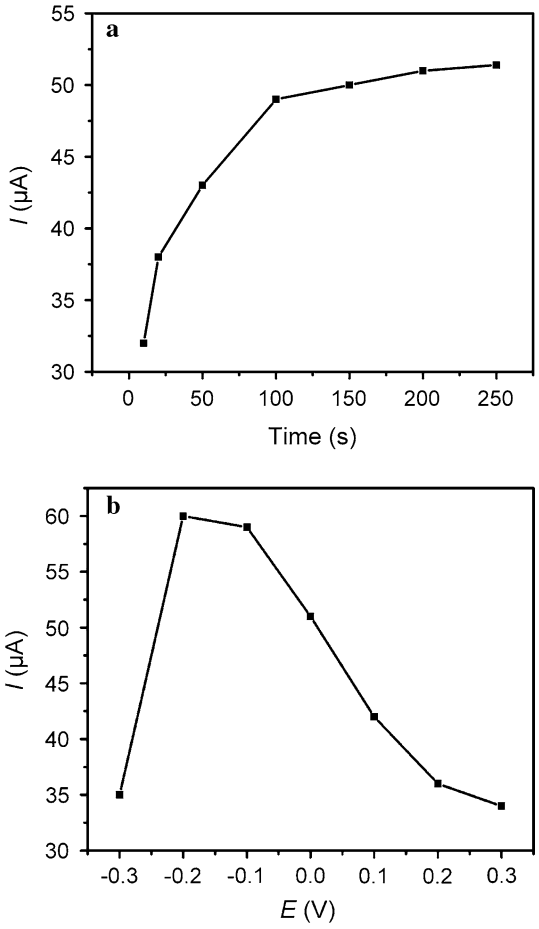

Fig. 5 **a** Effects of accumulation time on the oxidation peak current in 0.1 M PBS containing 25 μM BPA at pH 7.0. **b** Effects of accumulation potential on the oxidation peak current in 0.1 M PBS containing 25 μM BPA at pH 7.0. **c** The relationship between the peak potential (E_{pa}) and the natural logarithm of scan rate (ln$v$)

3.7 Effects of pH

The effect of pH value of PBS on the current response of RGO/M-GCE to BPA was investigated in the pH range of 5.54–8.91. As shown in Fig. 6a, the peak current slowly increased when the pH of the solution increased from 5.54 to 7.02, and then decreased with the further increase of pH. This showed that the protons participated in the reaction process of electrode [28]. As pH increased beyond 7.02, the residual carboxylic acid groups on the surface of RGO and BPA would be deprotonated and become anions. Due to the mutual repulsion between the negatively charged acidic

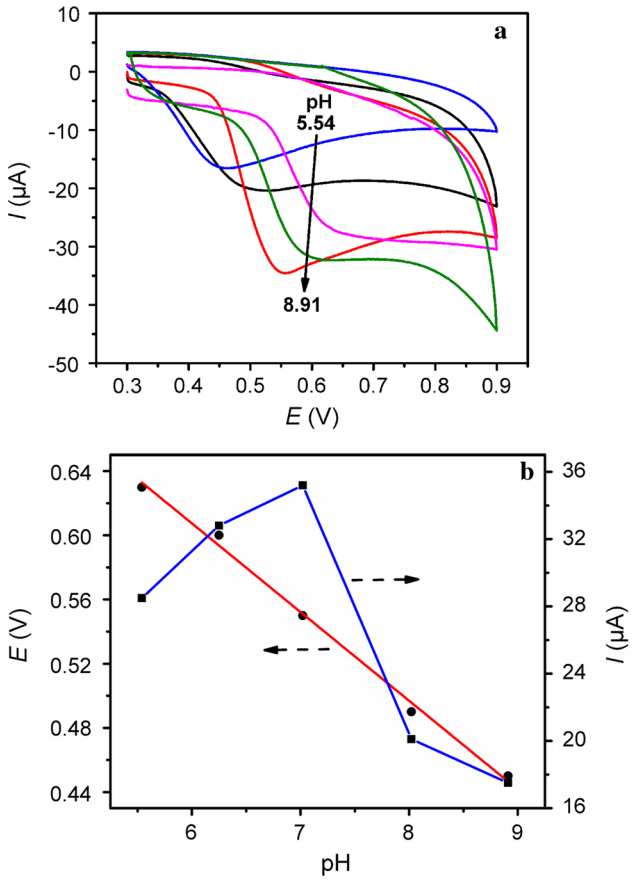

Fig. 6 **a** CV curves of 25 μM BPA at different pH: 5.54, 6.25, 7.02, 8.02, and 8.91 on RGO/M-GCE with the scan rate of 50 mV s^{-1}. **b** The relationship of the oxidation peak potential and current against pH

anions and BPA, the current response decreased. Considering the sensitivity of determination of BPA, pH 7.0 was chosen in the subsequent analytical experiments. The relationship between the oxidation peak potential (E_{pa}) and pH is also shown in Fig. 6b. It was found that the peak potential of RGO/GCE decreased with the increase of pH from 5.54 to 8.91. It obeyed the following equation:

$$E_{pa}(V) = -0.05528\ \mathrm{pH} + 0.9392. \quad (4)$$

The slope value (55.28 mV pH^{-1}) was very close to the theoretical value (57.6 mV pH^{-1}), indicating that the electron transfer was accompanied by the equal number of protons in the electrode reaction [29].

3.8 Electrochemical effective surface area and standard heterogeneous rate constant

The electrochemical effective surface areas (A) of bare GCE and RGO/M-GCE were investigated by chronocoulometry from 0 to 1.0 V. $K_3[Fe(CN)_6]$ was used as the model complex according to the following Anson equation:

$$Q(t) = 2nFAcD^{1/2}t^{1/2}/\pi^{1/2} + Q_{dl} + Q_{ads}, \quad (5)$$

where A is the surface area of working electrode, c is the concentration of substrate, Q_{dl} is the double layer charge which can be eliminated by background subtraction, Q_{ads} is the Faradaic charge, D is the diffusion coefficient, and other symbols have their usual meanings [30]. The experiment was carried out in $K_3[Fe(CN)_6]$ solution (1.0×10^{-4} M) containing 1.0 M KCl. The standard diffusion coefficient (D_0) of $K_3[Fe(CN)_6]$ is 7.6×10^{-6} cm^2 s^{-1} at 25 °C [31]. According to the results shown in Fig. 7a, the linear regression curves of $Q - t^{1/2}$ fit the following equations for bare GCE and RGO/M-GCE, respectively.

$$Q = 6.82 \times 10^{-6}t^{1/2} - 0.07 \times 10^{-6} \quad (6)$$

$$Q = 54.76 \times 10^{-6}t^{1/2} - 6.33 \times 10^{-6} \quad (7)$$

Based on the curves of Q versus $t^{1/2}$, A was calculated to be 0.0114 cm^2 and 0.0912 cm^2 for GCE and RGO/M-GCE, respectively. These results indicated that the effective surface area of the electrode remarkably increased after the electrode was modified. This increased the adsorption capacity of BPA due to the attraction between BPA and RGO/M. Then the enhanced current response and decreased detection limit were obtained.

The chronocoulometry experiments were carried out on RGO/M-GCE in 0.1 M PBS at pH 7.0 in the absence and presence of 2.5×10^{-8} M BPA, respectively. As shown in Fig. 7b, the plot of Q against $t^{1/2}$ showed a linear relationship after background subtraction. The linear regression curves of $Q - t^{1/2}$ accorded with the following equation:

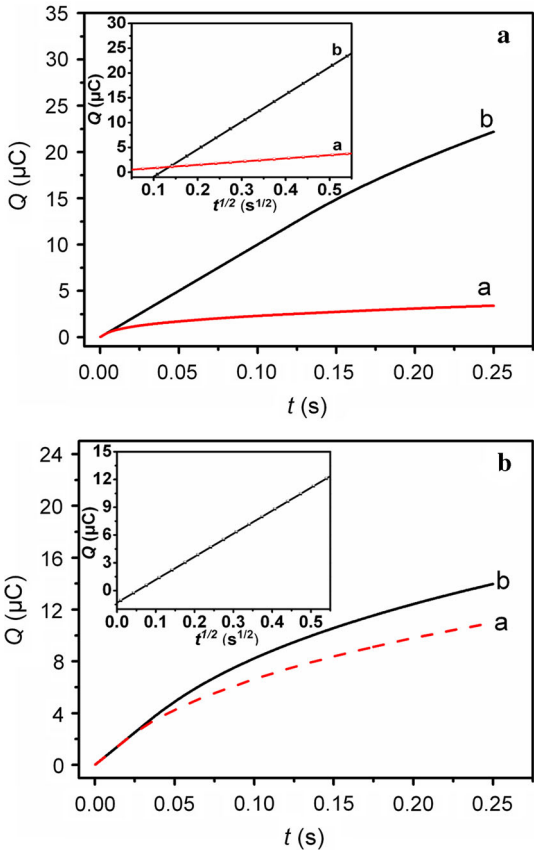

Fig. 7 **a** Plot of Q–t curves of (*a*) bare GCE, and (*b*) RGO/M-GCE in 0.1 mM $K_3[Fe(CN)_6]$ containing 1.0 M KCl. Insert: plot of Q–$t^{1/2}$ curves on (*a*) RGO/M-GCE and (*b*) bare GCE. **b** Plot of Q–t curves of the modified electrode in 0.1 M PBS at pH 7.0 in the presence (*a*), and absence (*b*) of 0.1 M BPA, respectively. Inset is the plot of Q–$t^{1/2}$ curve on RGO/M-GCE

$$Q = 24.85 \times 10^{-6}t^{1/2} - 1.31 \times 10^{-6} \quad (8)$$

The slope is 2.49×10^{-5}, and the intercept (Q_{ads}) is 1.31×10^{-6} C. D was calculated to be 2.5×10^{-5} cm^2 s^{-1} at 25 °C as $n = 2$, $A = 0.0912$ cm^2, and $c = 2.5 \times 10^{-4}$ M. The adsorption capacity, Γ_s, was calculated to be 5.95×10^{-6} mol cm^{-2} according to the following equation:

$$Q_{ads} = nFA\Gamma_s \quad (9)$$

The standard heterogeneous rate constant (k_s) for totally irreversible oxidation of BPA at the modified electrode was calculated according to the Velasco equation:

$$k_s = 2.415\exp(-0.02F/RT)D^{1/2}\left(E_{pa} - E_{pa/2}\right)^{-1/2}v^{1/2}, \quad (10)$$

where $E_{pa/2}$ represents the potential at which $I = I_{pa/2}$ in linear sweep voltammetry, D is diffusion coefficient, and other symbols have their usual meanings [32]. The k_s of

BPA was calculated to be about 9.1×10^{-3} cm s^{-1}. The standard heterogeneous rate constant (k_s) for totally irreversible oxidation of BPA at the modified electrode was found to be 2.65×10^{-3} cm s^{-1} [33]. The higher k_s of RGO/M-GCE could be attributed to the high adsorption capacity and conductivity of RGO/M. This suggested that RGO/M-GCE provided fast electron transfer between BPA and the surface of electrode.

3.9 Determination of BPA by differential pulse voltammetry

The determination of BPA on the RGO/M-GCE was performed using the differential pulse voltammetry technique (the quantification limit value (QL) for BPA was 0.01 μM) under the optimal conditions (pH 7.0, scan rate of 50 mV s^{-1}, accumulation time of 200 s, and accumulation potential of −0.2 V). As shown in Fig. 8a, the oxidation peak current of BPA increased when the concentration of BPA increased from 1.0×10^{-8} to 2.0×10^{-4} M. As shown in Fig. 8b, the calibration curve between the peak current (I) and the BPA concentration (c, 1.0×10^{-8}–2.0×10^{-4} M) could be described by the following equation:

$$I(\mu A) = 0.0969c + 14.83 (R = 0.9976) \quad (11)$$

The detection limit was estimated to be 4.0×10^{-9} M when signal-to-noise ratio (S/N) was 3. It was lower than those reported in previous studies (Table 1). The enhanced performance of RGO/M-GCE could be attributed to the combination of the excellent electrocatalytic properties of RGO and the electrostatic adsorption between the protonated M and BPA.

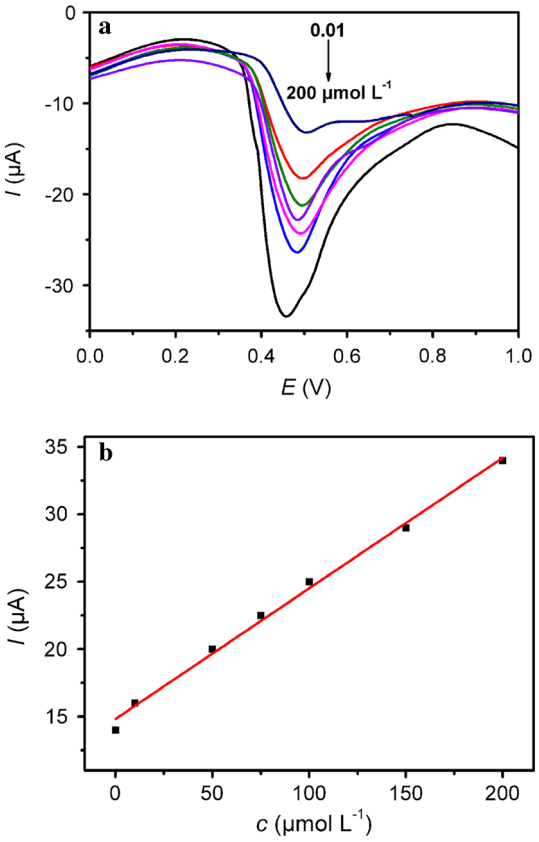

Fig. 8 **a** DPV curves of RGO/M-GCE in BPA solution at different concentrations (0.01, 10, 50, 75, 100, 150, and 200 μM, respectively). **b** Linear calibration curves

3.10 Reproducibility, stability, and interference

Reproducibility and stability are key elements for electrode performance. To prove the precision and practicability of the proposed method, the reproducibility of the RGO/M-GCE was investigated by cyclic voltammetry. The relative standard deviation was 1.9 % for the determination of 25 μM BPA after 20 successive measurements. This showed that the RGO/M-GCE had good reproducibility.

For the demonstration of the stability, the electrode was investigated by measuring the current response with 25 μM BPA every 2 weeks. Between measurements, the electrode was stored at 4 °C in a refrigerator. The response current of the electrode decreased to 96 % after 2 weeks. The electrode still retained 85 % of its original response even after 4 weeks. This indicated that the fabricated sensor had good stability. The good stability of RGO/M-GCE might be mainly attributed to the high thermal stability.

Under optimal conditions, the interference test was performed in the presence of 100-fold concentration of hydroquinone, phenol 4-nitrophenol, hydroxyphenol, ethanol, Mg^{2+}, Cu^{2+}, Ca^{2+}, Fe^{3+}, Al^{3+}, Zn^{2+}, SO_4^{2-}, and NO_3^-. The results showed that these organic compounds had no influences on the signals of BPA with deviations below 5 %. 100-fold concentration of above metal ions had no influences on the determination of 25 μM BPA.

3.11 Practical application

In order to confirm the performance of the fabricated sensor in practical applications, the BPA in the real samples (PVC food package, PC baby bottle, and PC water bottle) was detected. All samples were obtained from the local market. A standard addition method was used to evaluate the analytical performance of the sensor, and the results are summarized in Table 2. The recoveries were in the range of 97.00–100.96 %. This indicated that this method had good accuracy.

Table 1 Comparison of RGO/M-GCE sensor for determination of BPA with those reported

Sensors	Linear range (μM)	DL (μM)	References
MWCNT-GCE	0.02–20	0.0075	[17]
CS/Fe_3O_4-GCE	0.05–30	0.008	[18]
PAMAM/Fe_3O_4-GCE	0.01–3.07	0.005	[19]
NiTPPS/MWCNT-GCE	0.05–50	15	[20]
ITO electrode	5–120	0.29	[21]
Tyrosinase-CPE	1–20	0.15	[22]
RGO/M-GCE	0.01–200	0.004	This work

MWCNT multiwalled carbon nanotubes, *CS* Chitosan; *PAMAM* poly(amidoamine), *NiTPPS* Ni(II)tetrakis(4-sulfonatophenyl) porphyrin, *CPE* carbon paste electrode

Table 2 Determination of BPA in real plastic samples

Sample	Measured (μM)	Added (μM)	Found (μM)	Recovery (%)
PC bottle	4.67	10.00	14.23	97.00
PVC food package	5.52	10.00	15.67	100.96
PVC bottle	4.85	10.00	14.98	100.87
PC baby bottle	2.45	10.00	12.33	99.03

4 Conclusions

A sensitive and reliable electrochemical sensor was developed for the determination of BPA based on RGO/M-modified glass carbon electrode. Due to the combination of the excellent electrocatalytic property of RGO and the electrostatic attraction of protonated M, the modified electrode exhibited the enhanced performance on the oxidation of BPA. Under the optimal conditions, good linearity was observed between the differential pulse voltammetric peak current and the concentration of BPA in the range of 1.0×10^{-8}–2.0×10^{-4} M in PBS at pH 7.0 with the detection limit of 4.0×10^{-9} M ($S/N = 3$). The fabricated sensor was successfully applied in determining BPA in real plastic samples with good recoveries (97.00–100.96 %). Moreover, the sensor showed remarkable stability and reproducibility. Compared with many other reported electrochemical sensors, the new sensor possessed higher sensitivity and faster response.

Acknowledgments This study was funded by the National Natural Science Foundation of China (No. 51202020, 51472035), the Science and Technology Department of Jiangsu Province (BY2012099, BY2013024-04, BE2014089), Jiangsu Key Lab of Advanced Catalytic Materials and Technology (BM2012110), and the Qing Lan Project of Jiangsu Province of China.

Conflict of interest The authors declare that they have no conflict of interest.

References

1. Alkasir RS, Ganesana M, Won YH, Stanciu L, Andreescu S (2010) Enzyme functionalized nanoparticles for electrochemical biosensors: a comparative study with applications for the detection of bisphenol A. Biosens Bioelectron 26:43–49. doi:10.1016/j.bios.2010.05.001
2. Ballesteros-Gómez A, Rubio S, Pérez-Bendito D (2009) Analytical methods for the determination of bisphenol A in food. J Chromatogr A 1216:449–469. doi:10.1016/j.chroma.2008.06.037
3. Segner H, Caroll K, Fenske M, Janssen CR, Maack G, Pascoe D, Chafers C, Vandenbergh GF, Watts M, Wenzel A (2003) Identification of endocrine-disrupting effects in aquatic vertebrates and invertebrates: report from the European IDEA project. Ecotoxicol Environ Saf 54:302–314. doi:10.1016/S0147-6513(02)00039-8
4. Soto AM, Sonnenschein C (2010) Environmental causes of cancer: endocrine disruptors as carcinogens. Nat Rev Endocrinol 6:363–370. doi:10.1038/nrendo.2010.87
5. Chang CM, Chou CC, Lee MR (2005) Determining leaching of bisphenol A from plastic containers by solid-phase microextraction and gas chromatography–mass spectrometry. Anal Chim Acta 539:41–47. doi:10.1016/j.aca.2005.03.051
6. Nerin C, Philo MR, Salafranca J, Castle L (2002) Determination of bisphenol-type contaminants from food packaging materials in aqueous foods by solid-phase microextraction-high-performance liquid chromatography. J Chromatogr A 963:375–380. doi:10.1016/S0021-9673(02)00554-X
7. Kuramitz H, Matsushita M, Tanaka S (2004) Electrochemical removal of bisphenol A based on the anodic polymerization using a column type carbon fiber electrode. Water Res 38:2331–2338. doi:10.1016/j.watres.2004.02.023
8. Yin H, Zhou Y, Ai S, Han R, Tang T, Zhu L (2010) Electrochemical behavior of bisphenol A at glassy carbon electrode modified with gold nanoparticles, silk fibroin, and PAMAM dendrimers. Microchim Acta 170:99–105. doi:10.1007/s00604-010-0396-z
9. Chauke V, Matemadombo F, Nyokong T (2010) Remarkable sensitivity for detection of bisphenol A on a gold electrode modified with nickel tetraamino phthalocyanine containing Ni–O–Ni bridges. J Hazard Mater 178:180–186. doi:10.1016/j.jhazmat.2010.01.061
10. Zhu J, Chen S, Zhou H, Wang X (2012) Fabrication of a low defect density graphene-nickel hydroxide nanosheet hybrid with

enhanced electrochemical performance. Nano Res 5:11–19. doi:10.1007/s12274-011-0179-9
11. Yuan J, Zhu J, Bi H, Meng X, Liang S, Zhang L, Wang X (2013) Graphene-based 3D composite hydrogel by anchoring Co3O4 nanoparticles with enhanced electrochemical properties. Phys Chem Chem Phys 15:12940–12945. doi:10.1039/C3CP51710A
12. Cai YY, Li H, Du B, Yang MH, Li Y, Wu D, Zhao YF, Dai YX, Wei Q (2011) Ultrasensitive electrochemical immunoassay for BRCA1 using BMIM BF4-coated SBA-15 as labels and functionalized graphene as enhancer. Biomaterials 32:2117–2123
13. Lu CH, Yang HH, Zhu CL, Chen X, Chen GN (2009) A graphene platform for sensing biomolecules. Angew Chem 121: 4879–4881. doi:10.1002/ange.200901479
14. Ao ZM, Peeters FM (2010) Electric field activated hydrogen dissociative adsorption to nitrogen-doped graphene. J Phys Chem C 114:14503–14509. doi:10.1021/jp103835k
15. Ntsendwana B, Mamba BB, Sampath S, Arotiba OA (2012) Electrochemical detection of bisphenol A using graphene-modified glassy carbon electrode. Int J Electrochem Sci 7:3501–3512
16. Wang Q, Wang Y, Liu S, Wang L, Gao F, Gao F, Sun W (2012) Voltammetric detection of bisphenol a by a chitosan–graphene composite modified carbon ionic liquid electrode. Thin Solid Films 520:4459–4464. doi:10.1016/j.tsf.2012.02.069
17. Lu S, Fei J, He Q, Hu S (2004) Application of a multi-wall carbon nanotubes film coated electrode for the determination of bisphenol A leached from plastic waste samples. Chem Anal 49:607–617
18. Yu C, Gou L, Zhou X, Bao N, Gu H (2011) Chitosan–Fe3O4 nanocomposite based electrochemical sensors for the determination of bisphenol A. Electrochim Acta 56:9056–9063. doi:10.1016/j.electacta.2011.05.135
19. Yin H, Cui L, Chen Q, Shi W, Ai S, Zhu L, Lu L (2011) Amperometric determination of bisphenol A in milk using PAMAM–Fe3O4 modified glassy carbon electrode. Food Chem 125: 1097–1103. doi:10.1016/j.foodchem.2010.09.098
20. Liu X, Feng H, Liu X, Wong DK (2011) Electrocatalytic detection of phenolic estrogenic compounds at NiTPPS/carbon nanotube composite electrodes. Anal Chim Acta 689:212–218. doi:10.1016/j.aca.2011.01.037
21. Li Q, Li H, Du GF, Xu ZH (2010) Electrochemical detection of bisphenol A mediated by [Ru(bpy)3]2+ on an ITO electrode. J Hazard Mater 180:703–709. doi:10.1016/j.jhazmat.2010.04.094
22. Andreescu S, Sadik OA (2004) Correlation of analyte structures with biosensor responses using the detection of phenolic estrogens as a model. Anal Chem 76:552–560. doi:10.1021/ac034480z
23. Hummers WS Jr, Offeman RE (1958) Preparation of graphitic oxide. J Am Chem Soc 80:1339–1342. doi:10.1021/ja01539a017
24. He G, Chen H, Zhu J, Bei F, Sun X, Wang X (2011) Synthesis and characterization of graphene paper with controllable properties via chemical reduction. J Mater Chem 21:14631–14638. doi:10.1039/C1JM12393A
25. Kuramitz H, Nakata Y, Kawasaki M, Tanaka S (2001) Electrochemical oxidation of bisphenol A. Application to the removal of bisphenol A using a carbon fiber electrode. Chemosphere 45(1):37–43. doi:10.1016/S0045-6535(01)00032-7
26. Bard AJ, Faulkner LR (1980) Electrochemical methods: fundamentals and applications, 2nd edn. Wiley, New York
27. Cao Q, Zhao H, Zeng L, Wang J, Wang R, Qiu X, He Y (2009) Electrochemical determination of melamine using oligonucleotides modified gold electrodes. Talanta 80:484–488
28. Yin H, Zhou Y, Xu J, Ai S, Cui L, Zhu L (2010) Amperometric biosensor based on tyrosinase immobilized onto multiwalled carbon nanotubes-cobalt phthalocyanine-silk fibroin film and its application to determine bisphenol A. Anal Chim Acta 659:144–150. doi:10.1016/j.aca.2009.11.051
29. Laviron E (1974) Adsorption, autoinhibition and autocatalysis in polarography and in linear potential sweep voltammetry. J Electroanal Chem 52:355–393. doi:10.1016/S0022-0728(74)80448-1
30. Velasco JG (1997) Determination of standard rate constants for electrochemical irreversible processes from linear sweep voltammograms. Electroanalysis 9:880–882. doi:10.1002/elan.1140091116
31. Gooding JJ, Praig VG, Hall EAH (1998) Platinum-catalyzed enzyme electrodes immobilized on gold using self-assembled layers. Anal Chem 70(11):2396–2402. doi:10.1021/ac971035t
32. Anson FC (1964) Application of potentiostatic current integration to the study of the adsorption of cobalt (III)-(ethylenedinitrilo) tetraacetate on mercury electrodes. Anal Chem 36:932–934. doi:10.1021/ac60210a068
33. Velasco JG (1997) Determination of standard rate constants for electrochemical irreversible processes from linear sweep voltammograms. Electroanalysis 9(11):880–882. doi:10.1002/elan.1140091116